American Mineralogist, Volume 92, pages 1531–1534, 2007

LETTER

Novel 2:1 structure of phyllosilicates formed by annealing Fe^{3+}, Mg-rich dioctahedral mica

TOSHIHIRO KOGURE,[1,*] JUN KAMEDA,[1] AND VICTOR A. DRITS[2]

[1]Department of Earth and Planetary Science, Graduate School of Science, The University of Tokyo, 7-3-1 Hongo, Bunkyo-ku, Tokyo, 113-0033, Japan
[2]Geological Institute of the Russian Academy of Sciences, Pyzhevsky per 7, Moscow, Russia

ABSTRACT

A new modification of the 2:1 phyllosilicate layer has been discovered in annealed celadonite, a Fe^{3+}, Mg-rich dioctahedral mica. Plan-view diffraction patterns in TEM indicate a base-centered supercell with $A = 3a$ and $B = b$, where a and b are the cell dimensions of the original mica. Basic $h0l$ reflections with $h = 3n$ form an orthogonal lattice with one-layer periodicity, which is not expected for normal micas. The high-resolution TEM image along the <100> or related directions is similar to that expected from normal micas but the image along the <010> directions is completely different. From these images, it is concluded that the two tetrahedral sheets in a 2:1 layer are facing each other with no lateral $a/3$ stagger. In the proposed model that explains the high-resolution TEM images, two thirds of the spaces surrounded by two facing tetrahedral six-member rings accommodate three (Fe^{3+},Mg) cations and one third of the spaces are completely vacant. The (Fe^{3+},Mg) cations are coordinated by six or five oxygen atoms forming trigonal prisms or square pyramids, respectively.

Keywords: Crystal structure, electron microscopy, electron diffraction, mica, phase transition, phyllosilicates

INTRODUCTION

The 2:1 or TOT (Tetrahedral-Octahedral-Tetrahedral) layer is one of the basic structural units for phyllosilicates or clay minerals, which occur universally and are abundant on the global surface. Pauling (1930) was the first to determine the structure of the 2:1 layer by X-ray structure analysis and to report its di- and trioctahedral variation by pointing out the counterpart minerals, such as pyrophyllite and talc, muscovite and phlogopite, etc. About half a century later another variation in the dioctahedral 2:1 layer was reported (Tsipursky and Drits 1984). There are two kinds of octahedral sites (*cis* and *trans* sites) in the octahedral sheet, depending on the location of coordinating hydroxyls. The structure is called "*trans*-vacant" or "*cis*-vacant" depending on whether the octahedral vacancy is in the *trans* site or in one of two symmetrically independent *cis* sites (e.g., Drits 2003). Most dioctahedral 2:1 phyllosilicates are *trans*-vacant, but some illite and montmorillonite specimens were reported to have *cis*-vacant 2:1 layers. However, except for these variations in the octahedral site occupancy, the structure of the 2:1 layer is basically identical for all 2:1 phyllosilicates.

Dioctahedral 2:1 layers are topotactically dehydroxylated at elevated temperatures. Such dehydroxylation, as well as the dehydroxylated structure, was reported for pyrophyllite (Wardle and Brindley 1972), muscovite (Udagawa et al. 1974) and paragonite (Comodi and Zanazzi 2000). For instance, the dehydroxylation of muscovite is formulated as $KAl_2Si_3AlO_{10}(OH)_2 \rightarrow KAl_2Si_3AlO_{11} + H_2O$. As a result, aluminum becomes five-fold-coordinated with four apical oxygen atoms of the tetrahedral sheets and one residual oxygen atom that has the same z coordinate as aluminum (Wardle and Brindley 1972). These minerals are *trans*-vacant both in the natural state and in the dehydroxylated form. Drits et al. (1995) suggested that in the case of *cis*-vacant illite, dehydroxylation destabilizes aluminum in the *trans* site, which results in the migration of the aluminum to the vacant *cis* site. As a result the dehydroxylated 2:1 layer in *cis*-vacant illite is identical to that in dehydroxylated muscovite or *trans*-vacant illite.

On the other hand, celadonite and glauconite, dioctahedral micas with Fe^{3+} as the dominant octahedral cation, behave in a different way. They have *trans*-vacant structures in the natural state, and in the course of dehydroxylation by annealing, the octahedral cations migrate from the *cis* sites to the vacant *trans* sites (Tsipursky et al. 1985). Muller et al. (2000a) studied the structure of dehydroxylated celadonite and glauconite by fitting the experimental and calculated powder X-ray diffraction patterns. Furthermore, they reported the formation of supercells in dehydroxylated celadonite in the electron diffraction patterns along the layer normal (plan-view) in TEM (Muller et al. 2000b). They suggested that these supercells result from the long-range ordering in the octahedral cation distribution.

During a further investigation of these dehydroxylated celadonite samples using TEM, we have found that the supercell with triple length along the **a**-axis consists of 2:1 layers completely different from the normal ones. This paper describes the experimental results and proposes a structure model for this novel 2:1 layer.

SAMPLES AND METHODS

The sample investigated was a celadonite specimen named Z1 that has been investigated in several previous works (Drits et al. 1997; Muller et al. 2000a, 2000b). X-ray diffraction indicated that the specimen is completely monomin-

* E-mail: kogure@eps.s.u-tokyo.ac.jp

0003-004X/07/0809–1531$05.00/DOI: 10.2138/am.2007.2667

eral, which is not common for the celedonite specimens and suitable for the present experiment. The crystal-chemical formulae reported (Drits et al. 1997) is $(K_{0.89}Ca_{0.10})(Al_{0.05}Fe^{3+}_{0.96}Fe^{2+}_{0.26}Mg_{0.73})(Si_{3.94}Al_{0.06})O_{10}(OH)_2$.

The sample was heated in a furnace in air. The heating rate was 100 °C/h, and the sample was kept at 800 °C for 1 h and finally cooled at approximately –200 °C/h.

The specimen for cross-sectional TEM examination was prepared using the method of Kogure (2002). The specimen in powder form was embedded with epoxy resin between two glass slides. After hardening, the glass slides were cut using a diamond wheel to laths of ~1 mm thickness. The laths were thinned to ~50 µm by mechanical grinding and then argon ion milled. High-resolution transmission electron microscope (HRTEM) examination was performed at 200 kV using a JEOL JEM-2010. HRTEM images were recorded on films or with a Gatan MSC 794 bottom-mounted CCD camera. HRTEM images were taken at sufficiently thin regions of the specimen and by adjusting the defocus value, to record the contrast that corresponds to the projected potential of the crystal structure (Kogure 2002). Noisy contrast from amorphous materials in HRTEM images was removed using a Wiener-filter (Marks 1996; Kilaas 1998) developed by K. Ishizuka (HREM Research Inc.) and implemented with Gatan DigitalMicrograph version 3.1 0.0. A Gatan ES-500W CCD camera equipped at a port of the column just above the phosphor screen of the TEM was used to acquire diffraction patterns. X-ray chemical analysis in the TEM was performed using the JEOL EX-24025JGT energy-dispersive spectrometer (EDS) equipped to the TEM and the JEOL JED 2010 analysis program.

Multi-slice image simulation was performed using MacTempas (Total Resolution Co.). Images were simulated using parameters for the JEM-2010 electron microscope; viz. spherical aberration coefficient of 0.5 mm, spread of focus half width of 10 nm, beam convergence of 0.5 mrad, the objective aperture corresponded to 7.0 nm^{-1}, and acceleration voltage of 200 kV.

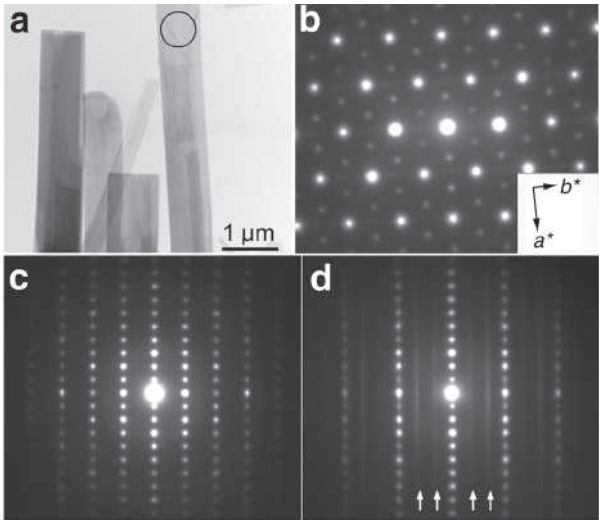

Figure 1. (**a**) Plan-view TEM image of Z1 celadonite. The circle indicates the aperture position to obtain the SAED pattern in **b**. (**b**) SAED pattern from the image in **a**. (**c**) SAED pattern along one of the X_i directions in a cross-sectional specimen. (**d**) SAED pattern along one of the Y_i directions, obtained by rotating the specimen by 30° about the **c***-axis.

Results and discussion

Figures 1a and 1b show a plan-view image and selected-area electron diffraction (SAED) pattern, respectively. The specimen is lath-shaped with the laths elongated along the ***a***-axis of the original 1*M* polytype. The SAED pattern shows weak reflections located between the intensive basic reflections and corresponding to the base-centered supercell with $A = 3a$ and $B = b$, where a and b are the cell dimensions for normal micas (Muller et al. 2000b). Weak streaks parallel to the **b***-axis are also observed, which was reported previously and ascribed to anti-phase domains (Muller et al. 2000b). Figures 1c and 1d are SAED patterns obtained from the cross-sectional specimen. Figure 1c shows the pattern along one of the X_i directions, and Figure 1d shows the pattern along one of the Y_i directions, obtained after rotating the specimen by 30° about the **c***-axis. See Bailey (1984) for the definition of X_i and Y_i (i = 1, 2, 3) directions. In most phyllosilicates with a base-centered cell, $a \cong 5.2$ Å and $b \cong 9.1$ Å, the X_i directions correspond to [100], [110] and [1$\bar{1}$0], and Y_i directions to [010], [310], and [3$\bar{1}$0]. These directions are expressed as [100], [130], and [1$\bar{3}$0] for X_i, and [010], [110], and [1$\bar{1}$0] for Y_i in the case of the supercell with $A = 3a$. First of all, we understand from these patterns that the crystal has one-layer periodicity along the stacking direction. The pattern in Figure 1c is almost similar to that along the [100] direction of 1*M* mica with the incident beam parallel to the mirror plane in the monoclinic system. The pattern in Figure 1d suggests that the crystal has a structure that is completely different from that of the normal micas. First, the reciprocal lattice rows (the white arrows) corresponding to the supercell ($h \neq 3n$) are completely streaked. Second, the reflections with $h = 3n$ that correspond to the basic cell form, surprisingly, an orthogonal reciprocal lattice. In normal micas, the polytype with one-layer periodicity is only 1*M* (monoclinic) and its diffraction patterns along any Y_i directions cannot be orthogonal.

Figure 2 shows HRTEM images along the X_i direction (2a) and the Y_i direction (2b), corresponding to the diffraction patterns in Figures 1c and 1d. The left part of each figure is the original image and the right part is the noise-reduced image obtained using the Wiener-filter. The contrast in Figure 2a is similar to that from normal 1*M* micas viewed along the <100> directions, as reported in several previous studies (e.g., Kogure and Nespolo 1999; Kogure 2002). Although celadonite in the natural state is a *trans*-vacant dioctahedral mica, the contrast in Figure 2a is rather close to that from trioctahedral micas (Kogure 2002). In contrast, the HRTEM image along the Y_i direction (Fig. 2b) is completely different from that from normal micas, or a normal 2:1 layer. As previously reported (Kogure 2002), a tetrahedral sheet is imaged as a row of dark spots, each of which corresponds to one SiO_4 tetrahedron, separated by about 2.6 Å (= a/2) when a TEM with ca. 2 Å point resolution is used. Therefore the positions of the tetrahedral sheets in the image can be identified, as indicated with "Si" in Figure 2. It is clear that the two tetrahedral sheets in a 2:1 layer are not staggered but aligned completely along the vertical direction. In addition, the presence of interlayer K cations requires a face-to-face arrangement of hexagonal cavities of adjacent tetrahedral sheets across the interlayers. Therefore the layers are stacked without any lateral shift in this structure (although Figs. 2a and 2b were not taken from the same region, we confirmed that the same contrast as that in Fig. 2b was observed when the region in Fig. 2a was rotated by 30° about the **c***-axis). Figure 2b also shows that the supercell with $A = 3a$ is formed by the contrast between the two tetrahedral sheets in a layer, probably by the particular distribution of (Fe^{3+},Mg) cations in the 2:1 layer. This contrast is considerably disordered along the stacking directions, as indicated by the white line. This disorder must correspond to the completely streaked pattern for $h \neq 3n$ reciprocal rows in Figure 1d.

Coexistence or interstratification of the new and normal 2:1 layers in a single grain was often observed in the specimen, implying that the transition is not complete from the annealing

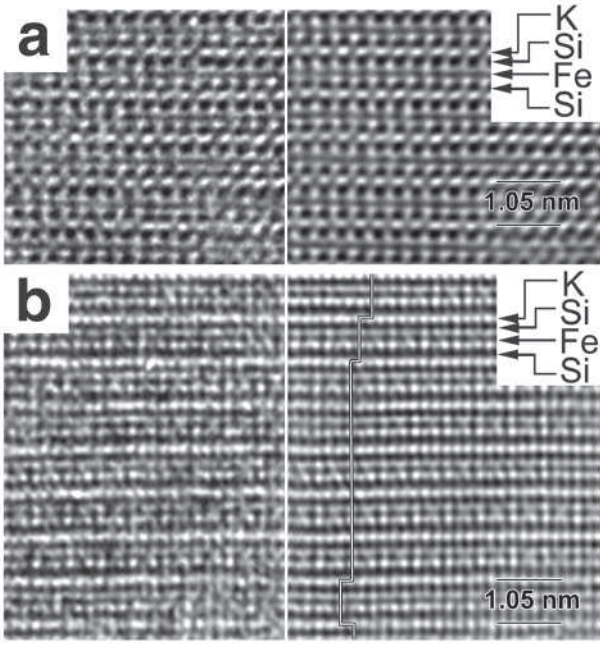

FIGURE 2. (**a**) HRTEM image along one of the X_i directions. The left is the original image and right is the one processed using the Wiener-filter. (**b**) HRTEM images along on of the Y_i directions. The white line around the center indicates stacking disorder with respect to the contrast of the supercell with 3*a* (see the text for the details).

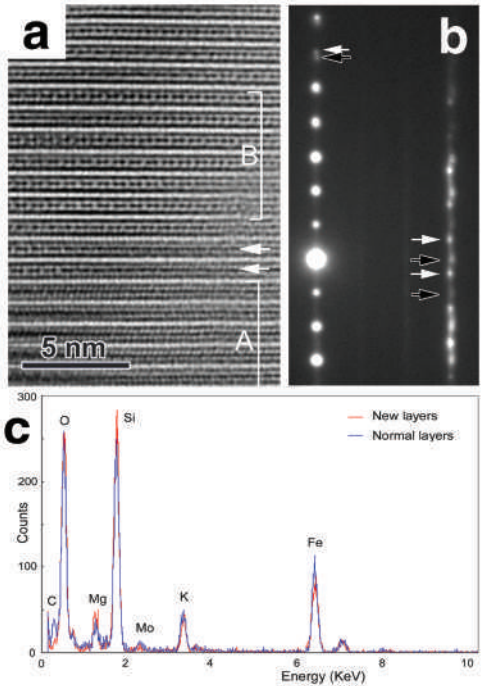

FIGURE 3. (**a**) HRTEM image along one of the Y_i directions, showing the coexistence of the normal 2:1 layers ("A") and new 2:1 layers ("B") in a grain. The layers indicated with the arrow contain both structures, alternating along the layer. (**b**) SAED pattern from the grain in **a**. The diffraction spots indicated with the white arrows are those from the normal 2:1 layers and spots with the black arrows are from the new 2:1 layers. (**c**) TEM-EDS spectra from the new 2:1 layers (red) and adjacent normal 2:1 layers (blue) in **a**. Molybdenum in the spectra is from the specimen-supporting ring.

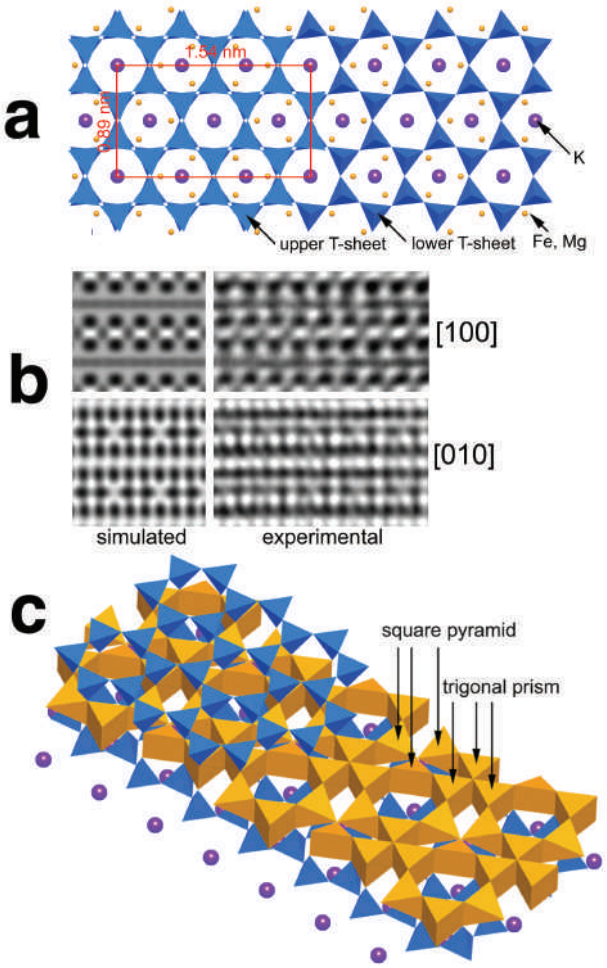

FIGURE 4. (**a**) A structure model of the new 2:1 layer, viewed along the layer normal. In the right half, the upper tetrahedral sheet is not displayed. The *z* coordinates of (Fe^{3+},Mg) cations are at the level of the center of the layer. (**b**) The comparison between the contrasts simulated from the model and the experimental image. The thickness and defocus values for the simulation are 25 and –350 Å, respectively. (**c**) Bird's-eye view of the structure model, with Fe^{3+},Mg cations shown as oxygen-coordinated polyhedra (see the text).

process. Figure 3a shows an example. The layers around the bottom of the figure (region "A") have the contrast of the normal 2:1 layer [stacking disorder with the $(2n + 1)60°$ layer rotation is observed (Kogure and Nespolo 1999)], whereas those around the center of the figure show the contrast of the new structure (region "B"). Two or three layers between regions "A" and "B" contain the two structures coexisting within the layer. The diffraction pattern from this grain is shown in Figure 3b. The diffraction spots indicated with the black arrows are from the new structure and those indicated with the white arrows are from the normal 2:1 layers. This pattern shows that the *b* parameter of the new layer is shorter than that of the normal 2:1 layer and d_{001} (= *c*) of the new layer is lengthened. Muller et al. (2000a) reported the cell dimension of sample Z1 annealed at 750 °C for 1 h. Using this cell dimension and the difference measured between diffraction

points corresponding to the two structures in the pattern in Figure 3b, the cell parameters of the new structure are estimated as a = 15.4, b = 8.9, c = 10.5 Å, and $\alpha = \beta = \gamma = 90°$. The large c value compared to normal mica is probably due to the slight increase in the distance between the non-staggered tetrahedral sheets in the layer along the **c**-axis.

X-ray chemical analysis at the regions "A" and "B" in Figure 3a has been performed using TEM-EDS, after recording the HRTEM image. No distinct difference in composition was detected between the two structures (Fig. 3c). As reported in the previous works (Heller-Kallai and Rozenson 1980; Muller et al. 2000c) celadonite was dehydroxylated and ferrous iron present in the natural state was oxidized by the present annealing process. Hence the composition of the annealed specimen is expressed approximately $K(Fe^{3+},Mg)_2Si_4O_{11}$. According to the result in Figure 3c, this composition can be applied to the new structure.

Because the upper and lower tetrahedral sheets are not staggered in the new structure, the formation of the octahedral sites between them is not expected and (Fe^{3+},Mg) must be coordinated by the oxygen atoms in some other way. We tried to find the location of (Fe^{3+},Mg) cations in the space between the two non-staggered tetrahedral sheets, which reproduces the HRTEM contrast in Figures 2a and 2b, through a trial-and-error procedure. Among several models examined, the most plausible one is shown in Figure 4a. Two thirds of the spaces in a 2:1 layer surrounded by the upper and lower tetrahedral six-member rings (termed hereafter "the hexagonal space") accommodate three cations whereas one-third of the hexagonal space is completely vacant. The z coordinate of these cations is at the level of the center of the 2:1 layer. Note that potassium atoms in Figure 4a are not within the 2:1 layer but in the interlayer region. The contrasts simulated for this model are compared with the experimental contrasts in Figure 4b. The characteristic contrast in the center of the 2:1 layer in the image along the Y_i direction (Fig. 2b), where four unequally spaced intense dark spots are observed in the supercell, is well reproduced in the simulated image. In this model, Fe^{3+} and Mg are randomly distributed.

In the case of normal dehydroxylated dioctahedral micas or pyrophyllite, one residual oxygen (Or) atom, which remains after the removal of a water molecule from the two hydroxyls, resides in the center of each hexagonal space and coordinates aluminum. As there is no cation in the vacant hexagonal space, Or atoms should be also absent there. Taking the stoichiometry $[K(Fe^{3+},Mg)_2Si_4O_{11}]$ into account, about a half of the occupied hexagonal spaces may accommodate two Or atoms and the other half accommodates one. Each Fe^{3+}, Mg cation is coordinated by four apical oxygen atoms of the lower and upper tetrahedral sheets. In the case of two Or atoms in the hexagonal space, it is likely that two Or atoms are located in the center of the space in the projection on the (001) plane and their z coordinates are in the apical oxygen plane. In this case, each cation has sixfold trigonal-prismatic coordination. In the case of only one Or atom, the atom is located in the center of the space, and each cation is fivefold-coordinated in a square pyramid (Fig. 4c). It is not clear at present whether the positions of these two kinds of hexagonal spaces with one or two Or atoms are distributed at random or ordered in accordance with the supercell of the structure.

The new 2:1 structure found in the present study, although an artificial product, is probably the first substantial modification of the 2:1 layer in phyllosilicates. The discovery of this structure will open new prospects for controlling the structure and properties of phyllosilicates and clay minerals. This structure may be also found in the dehydroxylated forms of other dioctahedral 2:1 phyllosilicates (e.g., ferripyrophyllite or nontronite) that have similar composition of the 2:1 layer. Further research should be directed at a more detailed characterization of this novel structure.

Acknowledgments

We are grateful to Bella B. Zviagina for some valuable comments. We also thank F. Nieto and F.J.M. Rietmeijer for their suggestions, which improved the manuscript. This work was partly supported by a Grant-in-Aid No. 17340160 [Section (B)] by the Japan Society for the Promotion of Science (JSPS). V.D. thanks Russian Foundation for Basic Research for support.

References cited

Bailey, S.W. (1984) Classification and structures of the micas. In S.W. Bailey, Ed., Micas, 13, p. 1–12. Reviews in Mineralogy, Mineralogical Society of America, Chantilly, Virginia.

Comodi, P. and Zanazzi, P.F. (2000) Structural thermal behaviour of paragonite and its dehydroxylate: a high-temperature single-crystal study. Physics and Chemistry of Minerals, 27, 377–385.

Drits, V.A. (2003) Structural and chemical heterogeneity of layer silicates and clay minerals. Clay Minerals, 38, 403–432.

Drits, V.A., Besson, G., and Muller, F. (1995) An improved model for structural transformations of heat-treated aluminous dioctahedral 2:1 layer silicates. Clays and Clay Minerals, 43, 718–731.

Drits, V.A., Dainyak, L.G., Muller, F., Besson, G., and Manceu, A. (1997) Isomorphous cation distribution in celadonite, glauconites and Fe-illites determined by infrared, Mössbauer and EXAFS spectroscopies. Clay Minerals, 32, 153–179.

Heller-Kallai, L. and Rozenson, I. (1980) Dehydroxylation of dioctahedral phyllosilicates. Clays and Clay Minerals, 28, 355–368.

Kilaas, R. (1998) Optimal and near-optimal filters in high-resolution electron microscopy. Journal of Microscopy, 190, 45–51.

Kogure, T. (2002) Investigation of micas using advanced TEM. In A. Mottana, F.P. Sassi, J.B. Thompson, Jr., S. Guggenheim, Eds., Micas: Crystal Chemistry and Metamorphic Petrology, 46, p. 281–312. Reviews in Mineralogy and Geochemistry, Mineralogical Society of America, Chantilly, Virginia.

Kogure, T. and Nespolo, M. (1999) First occurrence of a stacking sequence with (±60°, 180°) rotation in Mg-rich annite. Clays Clay Minerals, 47, 784–792.

Marks, L.D. (1996) Wiener-filter enhancement of noisy HREM images. Ultramicroscopy, 62, 43–52.

Muller, F., Drits, V.A., Plançon, A., and Besson (2000a) Dehydroxylation of Fe^{3+}, Mg-rich dioctahedral micas: (I) structural transformation. Clay Minerals, 35, 491–504.

Muller, F., Drits, V.A., Tsipursky, S.I., and Plançon, A. (2000b) Dehydroxylation of Fe^{3+}, Mg-rich dioctahedral micas: (II) cation migration. Clay Minerals, 35, 505–514.

Muller, F., Drits, V.A., Plançon, A., and Robert, J.-L. (2000c) Structural transformation of 2:1 dioctahedral layer silicates during dehydroxylation-rehydroxylation reactions. Clays and Clay Minerals, 48, 572–585.

Pauling, L. (1930) The structure of the micas and related minerals. Proceedings of National Academy of Science, 16, 123–129.

Tsipursky S.I. and Drits, V.A. (1984) The distribution of octahedral cations in the 2:1 layers of dioctahedral smectites studied by oblique-texture electron diffraction. Clay Minerals, 19, 177–193.

Tsipursky, S.I., Kameneva, M.Y., and Drits, V.A. (1985) Structural transformation of Fe^{3+}-conatining 2:1 dioctahedral phyllosilicates in the course of dehydroxylation. In J. Konta, Ed., 5th meeting of the European Clay Groups, Prague, 567–577.

Udagawa, S., Urabe, K., and Hasu, H. (1974) The Crystal structure of muscovite dehydroxylate. Japanese Association of Mineralogy, Petrology and Economic Geology, 69, 381–389.

Wardle, R. and Brindley, G.W. (1972) The crystal structures of pyrophyllite, 1*T*c and of its dehydroxylate. American Mineralogist, 57, 732–750.

Manuscript received April 12, 2007
Manuscript accepted April 26, 2007
Manuscript handled by Bryan Chakoumakos